Kinematically complete investigation of momentum transfer for single ionization in fast proton–helium collisions

Th Weber†, Kh Khayyat‡, R Dörner§, V Mergel†, O Jagutzki†, L Schmidt†, F Afaneh†, A Gonzalez‖, C L Cocke¶, A L Landers+ and H Schmidt-Böcking†

† Institut für Kernphysik, August-Euler-Straße 6, 60486 Frankfurt am Main, Germany
‡ Department of Physics, University of Missouri, Rolla, MO, USA
§ Fakultät für Physik, Universität Freiburg, Germany
‖ Centro Atomico Bariloche, 8400 S C de Bariloche, Argentina
¶ Department of Physics, Kansas State University, Manhatten, KS, USA
+ Department of Physics, Western Michigan University, Kalamazoo, MI, USA

Abstract. The dynamics of singly ionizing proton–helium collisions have been studied experimentally for several energies of the projectile (0.2, 0.5, 1.0 and 1.3 MeV) with the technique of cold target recoil-ion momentum spectroscopy (COLTRIMS). The complete final-state distribution in momentum space of all three particles was determined by measuring the three momentum components of the emitted electron and the coincident recoiling target ion. The momentum transfer and energy loss of the outgoing projectile was determined by momentum and energy conservation laws. Doubly differential cross sections of the kinematically complete experimental investigation are presented. The present data are compared with results from fast highly charged heavy-ion impact experiments.

1. Introduction

The understanding of kinematical details of the ionization processes by charged particle impact still remains a challenge in atomic physics. Great insights into the various contributing mechanisms have been gained from ionization cross sections doubly differential in kinetic energy and emission angle for the ejected electrons (see [1] for a review). However, a complete investigation of the collision dynamics describes the interaction of all particles before, during and after the ionization process. Due to their small mass and the significant role they play in molecular binding, the behaviour of the low-energy electrons has received most of the attention [2]. Until now there have only been a few sets of reliable data for the emission of low-energy (below 20 eV) electrons due to the experimental difficulties in measuring slow electrons with dispersive spectrometers [1, 3, 4]. Furthermore, kinematically complete investigations of ion–atom collisions are even more uncommon. These kinematically complete examinations provide nearly the whole information on the collision dynamics. Systematic and kinematically complete data have been available for electron impact, the so-called (e, 2e) processes, for many years [5]. Recently, such data have also became available for heavy ion impact [2, 6–8]. Considerable theoretical results for single differential cross sections (see, e.g., [9–14]) and fully differential cross sections [15, 16] have also became available within the last 15 years. These studies showed that even single ionization of atoms remains a challenge for experiment

and theory. To calculate or to measure the complete three-body kinematics of an ionizing ion–atom collision is very demanding.

Measurements of fully differential cross sections for the single ionization of helium differential in the momentum of electrons, recoiling ions and projectiles with swift incident protons at several energies are reported here (see [8, 17] for slow collisions). The measurements were carried out using the cold target recoil-ion momentum spectroscopy (COLTRIMS) technique (see [18] for a review). The momentum vectors (all three spatial dimensions) of the emitted electron and the recoil ion have been measured in coincidence. In addition, the charge state of the outgoing projectile has been determined in coincidence. The conservation of energy and momentum determined the energy loss and angular deflection of the projectile. We can therefore report on the kinematically complete measurement of helium-target single ionization by proton impact for several kinetic energies of the projectile. We use atomic units (au) throughout this paper ($m_e = \hbar = e = c/137 = 1$).

2. Experimental method

The experiment was performed at the 2.5 MV Van-de-Graaff accelerator of the Institut für Kernphysik of the University of Frankfurt. After passing the analysing magnet the beam was pulsed by the application of a 1 MHz square-wave transverse electric field along a set of 30 cm long deflecting parallel plates (the alternating voltage was ± 150 V). The electronic pulser/switcher was able to toggle from its positive to its negative maximum potential within 25 ns. After leaving the deflector the projectiles drifted 4 m before being scanned across an aperture with excursions of at least 1 cm. A set of two collimators generated a parallel beam with a diameter of about 0.5 mm (see figure 1). A coincidence between the pulsed beam measured with a position-sensitive multichannel-plate detector at the end of the beamline and the trigger signal of the electronic switcher allowed measurements of the time resolution of the beam chopping. We achieved a projectile bunch width of 1.5 ns FWHM, at a repetition rate of 2 MHz. The helium gas target was prepared in a pre-cooled one-stage supersonic jet [19, 20], which was placed perpendicular to the proton beam. The helium gas expanded through a
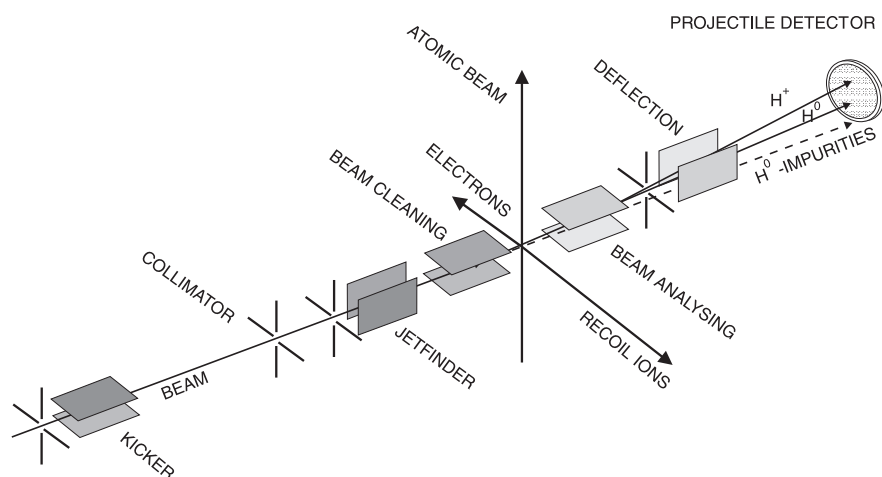

Figure 1. Schematic drawing of the beamline including the combined recoil-ion and electron momentum spectrometer.

30 μm nozzle, which was held at a temperature of 18 K forming a supersonic atomic beam. The jet diameter at the target region was about 1 mm with a density of $\approx 10^{11}$ atoms/cm^2. The pulsed ion beam and the atomic gas jet intersected at the centre of the combined recoil-ion and electron momentum spectrometer. The volume of this interaction region was below 1 mm^3. From the collision zone the recoiling target ions and electrons were extracted by a homogeneous electric field (60 V cm^{-1}) perpendicular to the plane of the incident beam and the target gas jet. After travelling through a short acceleration range (20 mm), the electrons were projected onto a position-sensitive detector. The recoiling ions passed through an electrostatic lens before drifting through a field-free region to another position-sensitive detector. This lens was optimized to eliminate the influence of the target spatial width on the momentum resolution of the recoil ions. All three detectors consisted of a multichannel plate z-stack combined with a wedge-and-strip anode [21]. From the position and time-of-flight, we derived the longitudinal and the transverse components of the final-state momentum of both electrons and recoiling ions. Due to the high extraction field, the recoil ions could be measured with a solid angle of 4π. The electron measurement had a solid angle of 4π for a longitudinal momentum of up to 1.2 au. The high electric field and pulse width of the proton beam resulted in a momentum resolution of 0.5 au for the recoil ions in all three dimensions. While the momentum resolution of the electrons in the electric-field direction (x-axis) comes to 0.5 au too, the resolutions along the other axis are better than 0.03 au. The outgoing projectiles were charge-state analysed. Due to the high beam intensity, the main beam could be steered away from the projectile detector but all electron transfer processes to the projectile have been recorded (see figure 1). More details concerning the apparatus and general aspects of recoil-ion momentum spectroscopy (RIMS) can be found in [18, 22–26].

3. Results and discussion

The method of COLTRIMS delivers the final state of target ionization in a nine-dimensional momentum space. Therefore, one obtains the square of a three-particle wavefunction in the continuum. In order to discern the collision dynamics, we classify the data into three independent planes as described below, and we show projections of the momentum vectors of all three particles onto these planes. The incident projectile moves along the longitudinal direction (z-axis). The direction of the transverse momentum transferred to the incoming projectile during the collision defines the x-axis (see figure 2). Thus the incoming and the scattered projectile defines the collision plane (x–z plane). The y-direction points out of this plane. The x–y plane is the so-called azimuthal plane. The plane perpendicular to the collision and azimuthal plane is a side view of the scattering process (i.e. the y–z plane). With these definitions we follow in principle the work of Moshammer *et al*, who first introduced these useful geometrical conventions (see [7]).

The energy and momentum transfer to the target system is very small compared with the initial energy and momentum of the incident particle in the laboratory system. Consequently, the longitudinal and the transverse momentum transfers are kinematically decoupled. The longitudinal momentum exchange is governed by the Q-value (see also equation (3)) or the inelasticy of the collision. The transverse direction represents the full transverse momentum balance and therefore shows the full three-body dynamics of the reaction.

As mentioned before, the loss of momentum of the incident proton and the momentum transfer in the transverse direction to the projectile is calculated via momentum and energy
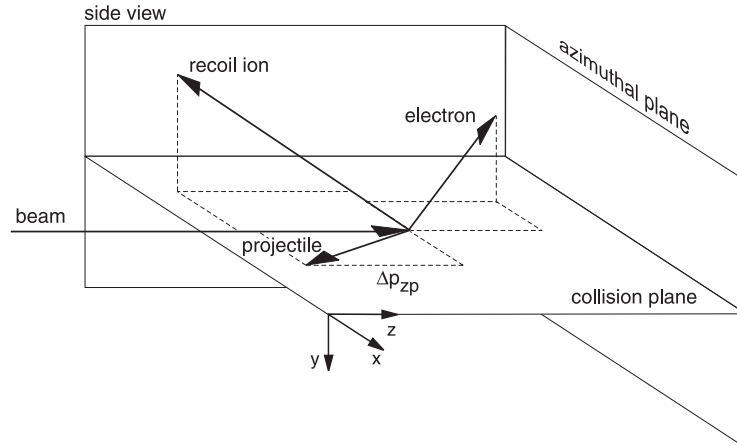
Figure 2. Definition of the three independent internal planes and coordinates used throughout this paper. For the projectile only the change in longitudinal momentum Δp_{zp} is relevant.

conservation. It is straightforward to derive the following:

$$\Delta p_{P\parallel} = -(Q + E_e)/v_P \tag{1}$$

$$\Delta p_{P\perp} = \vartheta_P \sqrt{2M_P E_P} \tag{2}$$

$$Q = \left(E_f^{\text{bind}} - E_i^{\text{bind}} \right) \tag{3}$$

where M_P is the projectile ion mass, E_P is the kinetic energy of the projectile, E_e is the kinetic energy of the electron, ϑ_P is the polar projectile scattering angle, v_P is the projectile velocity and Q is the inelasticity of the collision, i.e. the total difference in electronic energies between initial and final atomic states.

In the following we present the longitudinal momentum distribution first. After that we will show the results of momentum transfer in the transverse direction. Finally, we will present the whole momentum space with its projections as defined previously.

3.1. Longitudinal direction

The measured cross section differential in longitudinal momenta is shown in figure 3 for two different kinetic energies of the incident proton ((*a*) 1.3 MeV and (*b*) 200 keV; experimental results for a kinetic energy of 1.0 MeV can be found in [27]). The final momentum distributions of the electrons and the recoiling ions as well as the distribution of the loss in momentum of the projectiles are displayed (see also [17, 26, 28]). The experimental results were normalized to the total cross sections of Shah and Gilbody [29]. The authors give an absolute error of 17% for their data. While the recoil ions stay nearly at rest, the majority of the electrons are scattered in the forward direction (figure 3(*a*)). Both the electron and recoil-ion momentum distributions are very symmetric in shape. The momentum transfer to the target system is balanced by the loss in momentum of the proton. The spike-like shape of the proton momentum distribution is very asymmetric with a tail on the left-hand side of the projectile spectrum, which represents the electronic energy distribution E_e/v_p in computation of the change in momentum of the projectile (see equation (1)). This distribution represents the stopping power of the protons in a helium gas-target measured with a resolution of $\Delta p_{\parallel}/p = 7.5 \times 10^{-6}$. With decreasing velocity of the proton, the number of electrons emitted with higher momentum in the forward
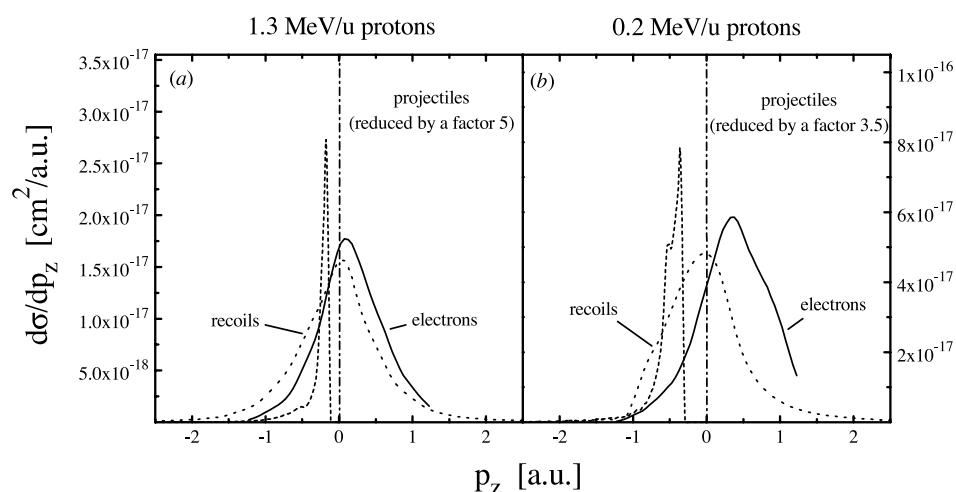
Figure 3. Experimental longitudinal momentum distributions of the recoil ions (dotted curve), electrons (full curve) and the loss in momentum of the protons (broken curve) for two different kinetic energies of the incident projectile: (*a*) 1.3 MeV u^{-1} and (*b*) 0.2 MeV u^{-1}. The loss of momentum of the proton is calculated via energy and momentum conservation. The cuts in the electron distributions are due to the small angular resolution (smaller than 4π).

direction is rising, which can be clearly seen in figure 3(*b*). As more momentum is transferred to the target system, the shape of the electron distribution becomes asymmetric, and the falling edge on the right-hand side is extended to the forward direction. This is due to the influence of post collision interaction (PCI) which refers to the long-range Coulomb potential of the outgoing projectile attracting the ionized electron in the forward direction and repelling the recoiling ion. The influence of the sign and the value of the projectile charge on the collision dynamics has been studied experimentally in [27, 30–34] and theoretically in [35–38]. At this point we want to emphasize that due to the extraction voltage of our spectrometer the detection solid angle of 4π for the electrons was limited to a momentum of 1.2 au. Thus it is possible that this broadening effect is much more dramatic than displayed here (the events detected with momenta larger than 1.2 au are not shown). While the momentum distribution of the recoil ions still peaks close to zero, the majority of the recoil ions are emitted in the backward direction. The shape of this dispersal becomes asymmetric, too. The upcoming shoulder seen in the rising edge on the left-hand side of the spectrum is not due to PCI but to another process called 'cusp' (electron capture to the continuum ECC of the projectile; for theoretical and experimental results see [39–44]. This aspect will be discussed in detail and separately in a future paper. On average, the electrons compensate nearly completely the mean momentum loss of the projectiles. For lower kinetic energy of the incident proton the momentum loss distribution of the projectile peaks at a larger value and the shape is broader than before. The sharp asymmetric structure is similar to the momentum loss spectrum at higher kinetic energy. Here the measured momentum exchange processes differ substantially from single ionization with very fast highly charged ions (see [7]). In that case the electron momentum is nearly completely compensated by the recoiling ion. In these very fast collisions the projectile merely transfers momentum to the target electron. The interaction can be described by a virtual photon field (Weizsaecker–Williams formalism [45]) where the target system absorbs virtual photons from the intense electromagnetic field produced by the passing ion.
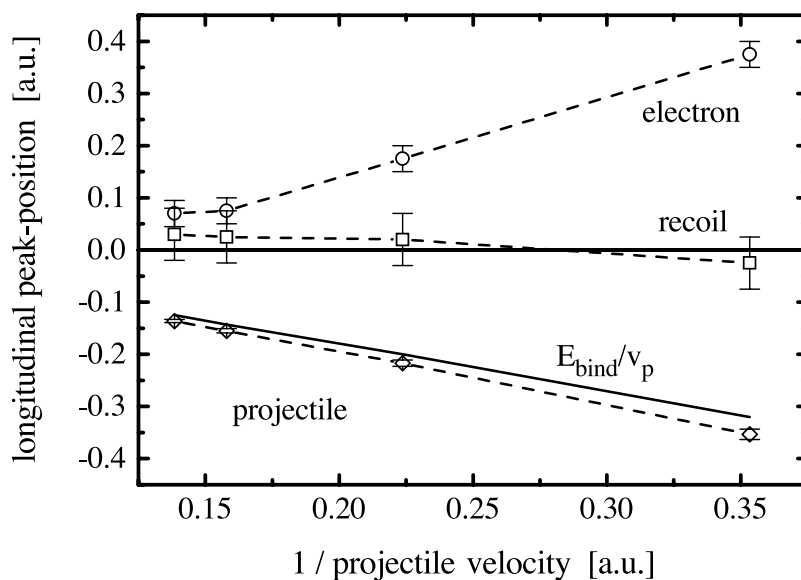
Figure 4. Peak positions of the longitudinal momentum of the fragments of the collision as a function of the reciprocal velocity of the incident protons. The peak position of the projectiles qualifies the mean momentum loss. The full curve defines the minimal loss in momentum of the incoming proton computed as E_{bind}/v_{p}.
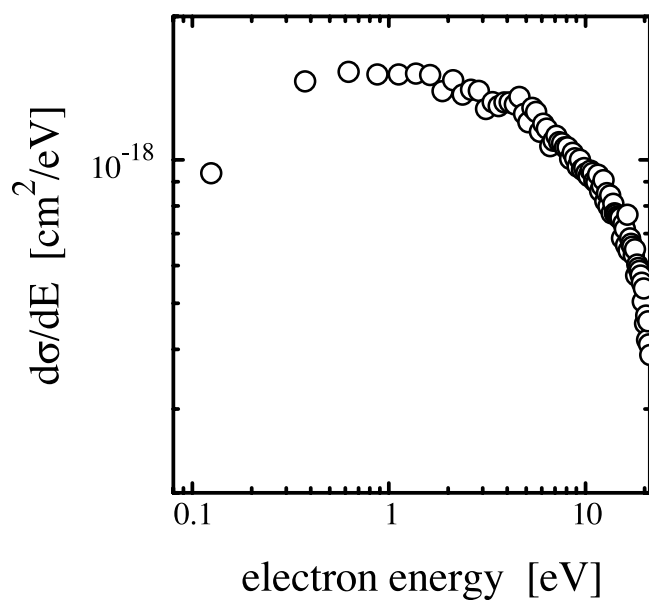

Figure 5. Cross section for the emission of electrons singly differential in electron energy for single ionization of helium with protons of a kinetic energy of 1 MeV u^{-1}. The statistical error bars are the same size as the circles.

Figure 4 shows the evolution of the peak position of the momentum distributions as a function of the reciprocal of the projectile velocity. We find a nearly linear dependence. This
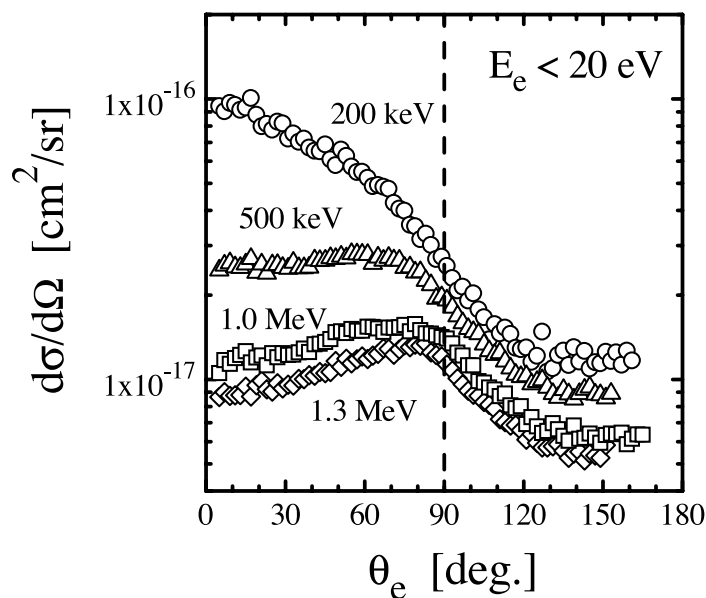
Figure 6. Singly differential cross section for the emission of low-energy electrons ($E_e < 20$ eV) as a function of the ejected electron's polar angle for four different kinetic energies (1.3, 1.0, 0.5 and 0.2 MeV) of the protons.

can be expected since the momentum transfer in a field is proportional to the collision time. The full curve defines the minimal loss in momentum for the projectiles computed by E_{bind}/v_p.

The singly differential cross section as a function of electron energy integrated over all emission angles is shown in figure 5. Most of the electrons are emitted with energies lower than 20 eV. The weak maximum around 1 eV might be an artefact resulting from our experimental resolution and needs further investigation. For these low-energy electrons the polar angle distribution is presented in figure 6 for several kinetic energies of the projectile. A definite preference of forward emission at slower proton velocity can be observed. For 200 keV impact energy of the projectile, the majority of the electrons peak at 0° and a difference of nearly one magnitude between forward and backward emission can be clearly seen. With increasing kinetic energy of the projectile, the electrons tend to escape under 90°.

3.2. Transverse direction

The cross sections singly differential in transverse momentum for all outgoing particles are displayed in figure 7. In this case, the kinetic energy of the incident proton beam was 500 keV. In the transverse direction the recoiling ion receives on average as much momentum as the electron, which is similar to the situation for single ionization by fast highly charged ions investigated by Moshammer *et al* [7]. However, the momentum transfer to the projectile is very different in these two cases. In single ionization with highly charged ions, the momentum transfer to the projectile is smaller than the observed momenta of the atomic fragments. In our case the incident proton undergoes a momentum exchange in the transverse direction, which is nearly equal to or even higher than that of each atomic fragment. This fact clearly shows that here the proton delivers most of the transverse momentum to the target atom, in contrast to the ionization with fast highly charged ions. This is similar to our findings in the
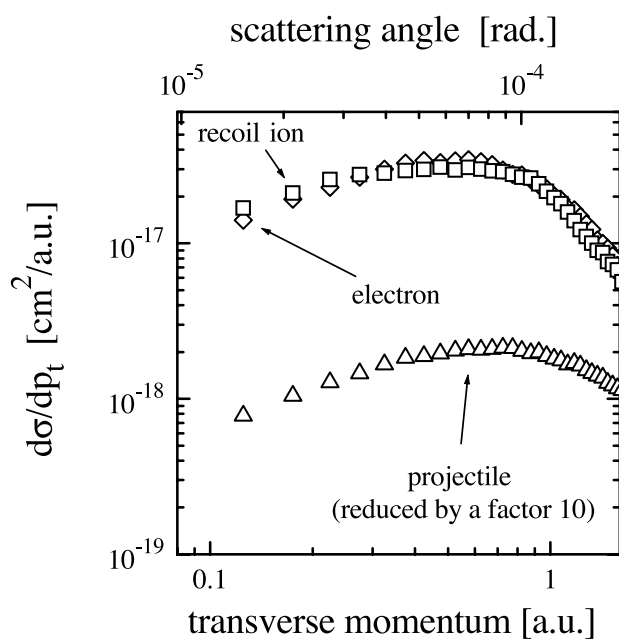
scattering angle [rad.]

Figure 7. Transverse momentum distributions of the recoiling ions (squares), electrons (diamonds) and projectiles (triangles) for single ionization of helium with protons (500 keV kinetic energy). The transverse projectile momentum is directly associated with the scattering angle (see the upper scale).

longitudinal direction presented in the previous section. When varying the kinetic energy of the incident proton, the relative distributions in transverse momentum of all particles involved in the collision do not vary significantly. For more than 99% of the total cross section the scattering angle of the projectile, which is directly connected to the transverse momentum of the proton, is always smaller than 0.5 mrad (see also [46, 47]).

In order to explore and understand the mechanisms leading to single ionization of the target, it is instructive to plot the azimuthal angle correlation between all particles. As described above, the transverse direction and therefore the angular distribution in the azimuthal plane reflects important information about the three-body dynamics. For that reason we plot the data as a function of the azimuthal angle between the recoil ion and projectile ϕ_{rp} versus the angle between the recoil ion and electron ϕ_{re}. The distribution (figure 8) has the shape of a triangle. Events localized along the three sides of the triangle correspond to three different two-body interactions. The right-hand side reflects all events where the electrons and the recoiling ions were emitted back-to-back, while the proton momentum is uncorrelated and therefore the azimuthal angle ϕ_{rp} can vary between 0° and 180°. This characterizes the dynamics of a photoionization process in which nearly no momentum is transferred to the target system and the atomic fragments compensate each other's momentum, resulting in back-to-back emission of the photo-electron and ion. The horizontal side on top of the triangle qualifies nucleus–nucleus interaction. Now the projectile and the recoil ion are emitted back-to-back with an azimuthal angle of $\phi_{rp} = 180°$ and the electron acts as a spectator. The diagonal defined as $\phi_{rp} = 180° - \phi_{re}$ represents the two-body interaction between the electron and the projectile. While the sides of the triangle qualify pure two-body interactions the pattern in between represents momentum exchange between all participating particles and therefore describes the
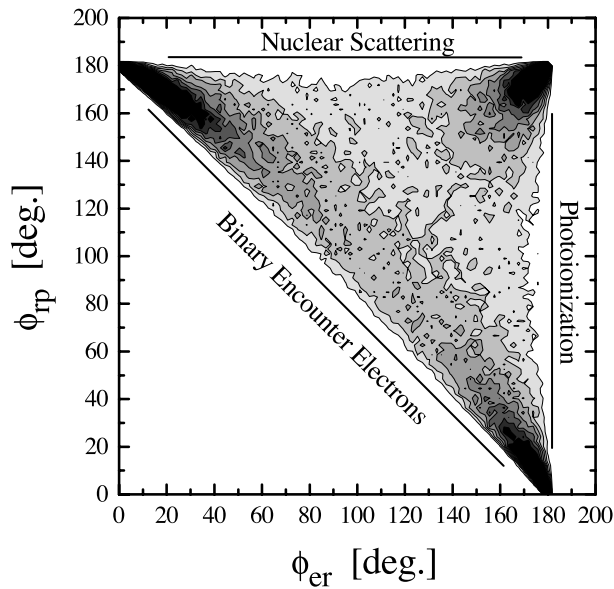
Figure 8. The azimuthal angle ϕ_{rp} between the recoil ion and the proton as a function of the azimuthal angle ϕ_{er} between the recoil ion and the electron for single ionization of helium with protons; the kinetic energy of the incident projectiles is 1.3 MeV u^{-1}. The three sides of the triangle show the locus of events which are dominated by one of the three possible two-body momentum exchange processes in which the third particle is not involved. Simple kinematical reasons prohibit events being outside of the triangle shaped distribution (for a better explanation see also the main text). The grey-scale of the doubly differential cross section $d^2\sigma/(d\phi_{rp}\,d\phi_{re})$ is linear.

dynamics of a correlated three-body system. Due to momentum and energy conservation, events outside of the triangle are forbidden. As displayed in figure 8 (for a kinetic energy of 1.3 MeV for the proton) binary-encounter collisions are the most probable processes leading to single ionization of the target atom. Lots of events are located at the corners of the triangle, which means that two particles always tend to emerge into the same transverse direction, while the remaining participant of the collision is scattered to the opposite side. The distribution shown in figure 8 is in striking contrast with the corresponding distribution for highly charged ion impact [7]. There, most of the counts are located along the $\phi_{re} = 180°$ line, indicating the dominance of dipole transitions (see also [2]).

3.3. Three-particle dynamics

In this section we will present double differential cross sections in momentum space of all outgoing particles of the collision. These data illuminate the complete three-body dynamics of atomic scattering processes. As mentioned before, it is instructive to show projections of the momentum vectors on three different orthogonal planes, which are defined as described above (see also figure 2). Figure 9 displays the momentum distribution of all reactants in the collision plane, which is defined by the incident and the outgoing proton. Thus per definition, all projectiles are emitted along the positive x-axis. The abscissa of this spectrum again shows the loss of momentum in the longitudinal direction for the proton Δp_{zp}. All the features described in the last two sections now can be clearly seen at a glance. It is evident that the proton exchanges significant momentum with the electron as well as with the target nucleus—the transverse
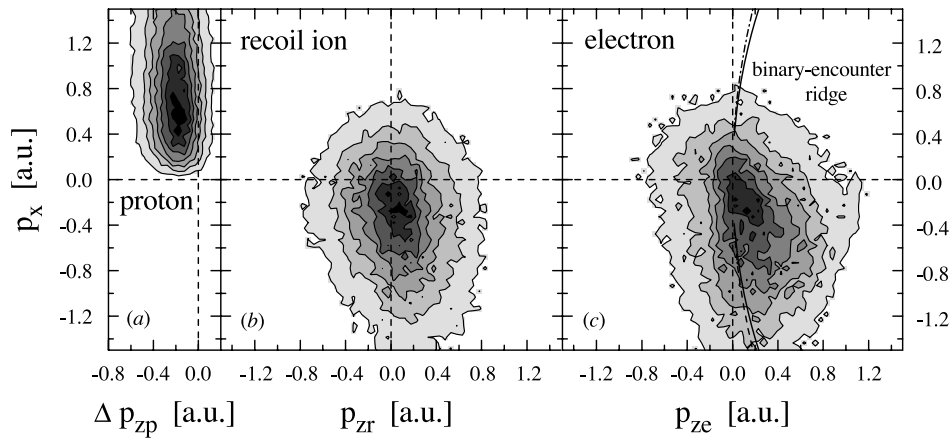
Figure 9. The momentum distribution for (*a*) the protons, (*b*) recoil ions and (*c*) electrons projected on the collision plane, which is defined by the incident and outgoing projectile. Thus per definition the proton is always scattered along the positive *x*-axis. The doubly differential cross section $d^2\sigma/(dp_x\,dp_z)$ (respectively $d^2\sigma/(dp_x\,dp_{\Delta z})$) is plotted on a linear scale. The curves in (*c*) indicate binary-encounter processes between the electron and the proton; the events along the full line take into account the loss of momentum due to the binding energy of the electron while the chain fraction of the circle neglects this fact.

momentum transfer to the projectile indicates the three-body interaction. Nevertheless, there are a certain number of events that show recoil-ion and electron emission in the same direction as the incident particle. The momentum distribution of the electron approaches the well known ridge of the binary-encounter processes, which are located on a circle around the velocity of the incident proton in figure 9(*c*). For events along this line the electron balances the main part of the momentum loss of the projectile, while the recoiling ion stays nearly at rest.

The interplay between the three particles can also be seen in the azimuthal plane shown in figure 10. Here the momentum vector of the incoming proton is perpendicular to the plane of the figure. In each figure the transverse momentum vector of one particle is fixed as indicated by the arrows, whose lengths are arbitrary. In the top row (figures 10(*a*) and (*b*)) the recoil ion is fixed and the transverse momentum of the projectile and the electron have been plotted, while in figure 10(*c*) the emission of the outgoing proton has been fixed and the electron momentum distribution is displayed. The interplay and accordingly the momentum transfer between all particles are clearly evident.

The last perspective shown is the so-called 'side view' of the atomic collision in momentum space (see figure 2). In figure 11 the projections of the momenta of the emitted recoil ion (*a*) and the scattered electron (*b*) onto the (*z*–*y*)-plane are presented while the outgoing momentum of the projectile is aligned along the *x*-axis. Thus per definition, the proton momentum vector stands perpendicular to the plane of the page. A narrow distribution around the longitudinal axis in figure 11(*b*) would therefore indicate a strong nucleus–nucleus interaction. That is clearly not the case; there are a certain number of events located outside the collision plane in momentum space. This fact also emphasizes that despite the importance of the two-body binary-encounter processes, the three-particle interaction contributes a large portion of the single-ionization cross section. This side view also illustrates the interaction between the electron and the projectile in the longitudinal direction and the influence of the post-collision interaction. The shape of the electron momentum distribution becomes more and more anisotropic with decreasing velocity of the incident projectile.
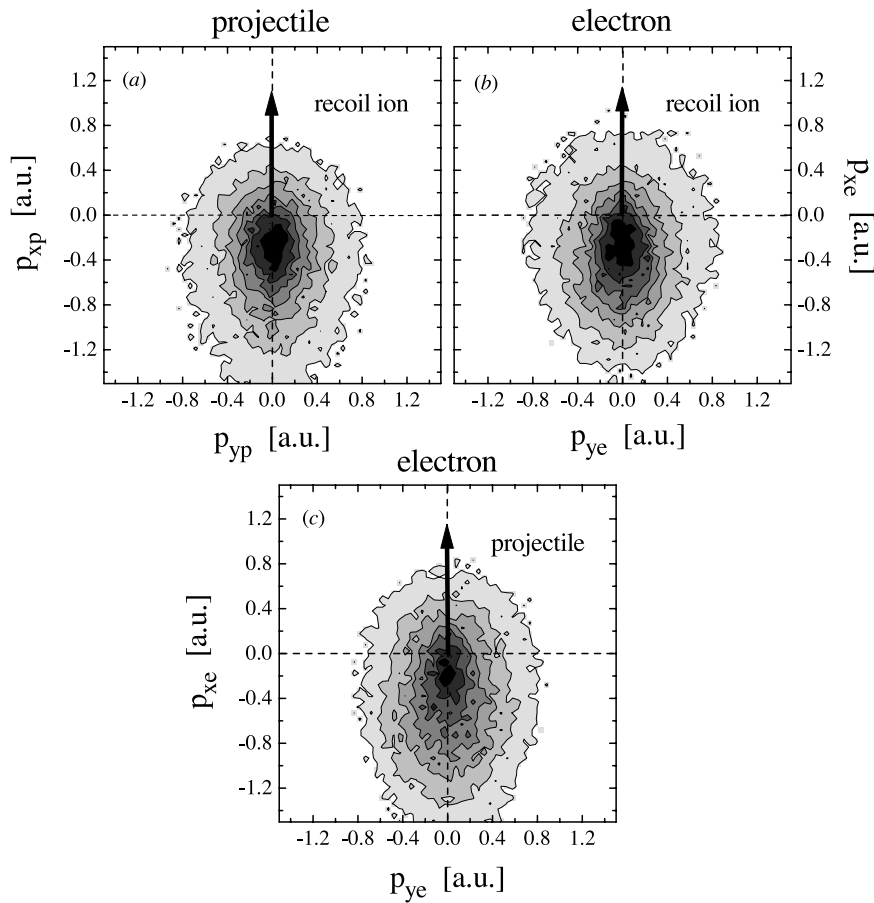
Figure 10. The momenta of the projectile (*a*) and of the electron (*b*) and (*c*) projected on the azimuthal plane, which stands perpendicular to the incident proton. The arrows indicate that one particle is fixed in one direction (no restriction to the value of its momentum) while the other ones can vary; for (*a*) and (*b*) the recoil ion goes along the positive *x*-axis, in (*c*) the projectile is fixed. The doubly differential cross sections $\mathrm{d}^2\sigma/(\mathrm{d}p_x\,\mathrm{d}p_y)$ are presented on a linear scale.

4. Conclusions

The COLTRIMS method has been applied successfully for the investigation of single ionization of helium by proton impact. We obtained a kinematically complete picture of the ionization dynamics for fast proton collision which is unprecedented in completeness and detail. This experiment fits in with the experimental studies of single ionization of helium with charged particles. It is a link between ionization by slow proton impact [48, 49] and single ionization by fast highly charged ions [2, 7].

Single ionization of helium proves to be caused by a highly complex interplay of interactions of a three-body system. Within the observed energy regime, the projectile appears to be directly responsible for the momentum distributions in the final state of the outgoing particles in contrast to collisions with fast highly charged particles. We find that each of the three two-body momentum exchange processes (interactions between projectile and electron, electron and recoil as well as projectile and target nucleus) play an important role in the
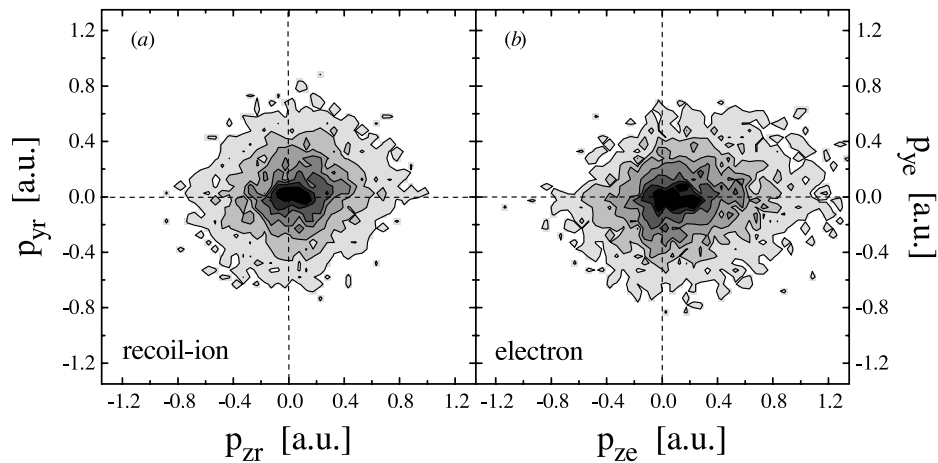
Figure 11. Projection of the momenta of (*a*) the outgoing recoil ion and (*b*) the emitted electron on the plane, which is orientated rectangular to the collision and azimuthal plane ('side view'). The momentum vector of the scattered projectile stands perpendicular to the paper plane. The doubly differential cross sections $\mathrm{d}^2\sigma/(\mathrm{d}p_x\,\mathrm{d}p_y)$ are presented on a linear scale.

intermediate projectile velocities investigated here. Binary encounter between projectile and electron, however, is most likely. Therefore, the majority of all recoil ions and electrons are emitted with small momentum, thus low-energy ($\leqslant 20$ eV) electrons dominate the cross section. The asymmetry in the longitudinal direction increases with decreasing kinetic energy of the incident proton. Within this regime of perturbation, the projectile transfers a definite momentum to the target system and an increase of the influence of post-collision interaction for decreasing projectile velocities can be clearly seen. In the longitudinal direction the required energy for ionization comes from the kinetic energy of the proton. The electrons mainly compensate the loss of momentum of the projectile; the recoiling ions remain spectators. The investigation of momentum transfer in the transverse direction clearly showed the importance of the interaction of the projectile. In comparison with single ionization of helium induced by fast highly charged ions, the electron recoil correlation does not play such an important role. The proton transfers momentum to the target atom in the longitudinal as well as in the transverse direction. Therefore, it determines the momentum distribution of the atomic fragments in the final state. The ratio of the projectile charge state to the velocity is a crucial quantity for predicting the mechanisms of ionization with charged particles and the dominant dynamics of three-body systems.

As could clearly be seen, all charged particles interact in the continuum and therefore this situation is an ideal example for the investigation of a three-body system. The contribution of the nuclear Coulomb interaction leading to ionization is relatively small. Due to this fact, it remains impossible to extract the impact parameter from the observed quantities (see also [47, 50, 51]).

Acknowledgments

References

[1] Rudd M E, Kim Y, Madison D H and Gay T J 1992 *Rev. Mod. Phys.* **64** 441
[2] Stolterfoht N, DuBois R D and Rivarola R D 1997 *Electron Emission in Heavy Ion–Atom Collisions* (Berlin: Springer)
[3] Stefani G 1987 *5th Int. Conf. on the Physics of Electronic and Atomic Collisions* ed H B Gilbody *et al* (Brighton: University Press) Abstracts p 163
[4] Tribedi L C, Richard P, Wang Y D, Lin C D and Olson R E 1996 *Phys. Rev. Lett.* **77** 3767
[5] McCarthy I E and Weigold E 1991 *Rep. Prog. Phys.* **54** 789
[6] Kravis S D *et al* 1996 *Phys. Rev.* A **54** 1394
[7] Moshammer R, Ullrich J, Kollmus H, Schmitt W, Unverzagt M, Schmidt-Böcking H, Wood C J and Olson R E 1997 *Phys. Rev.* A **56** 1351
[8] Dörner R, Khemliche H, Prior M H, Cocke C L, Gary J A, Olson R E, Mergel V, Ullrich J and Schmidt-Böcking H 1996 *Phys. Rev. Lett.* **77** 4520
[9] Fainstein P D, Ponce V H and Rivarola R D 1991 *J. Phys. B: At. Mol. Opt. Phys.* **24** 3091–119
[10] Horbatch M and Dreizler R M 1985 *Phys. Rev.* A **113** 251
[11] Olson R E, Ullrich J and Schmidt-Böcking H 1989 *Phys. Rev.* A **39** 5572
[12] Fang X and Reading J F 1991 *Nucl. Instrum. Methods* B **53** 453
[13] McGuire J H, Müller A, Schuch B, Groh W and Salzborn E 1987 *Phys. Rev.* A **35** 2479
[14] Salin A *et al* 1987 *Phys. Rev.* A **36** 5471
[15] Fukuda U, Shimamura I, Vegh L and Watanabe T 1991 *Phys. Rev.* A **44** 1565
[16] Salin A *et al* 1991 *J. Phys. B: At. Mol. Opt. Phys.* **24** 3211
[17] Wang Y D, Rodriguez V D, Lin C D, Cocke C L, Kravis S, Abdallah M and Dörner R 1996 *Phys. Rev.* A **53** 3278
[18] Dörner R, Mergel V, Jagutzki O, Spielberger L, Ullrich J, Moshammer R and Schmidt-Böcking H 2000 *Phys. Rep.* **330** 95–192
[19] Miller D R 1988 Free jet sources *Atomic and Molecular Beam Methods* ed G Scoles (Oxford: Oxford University Press) p 14
[20] Brusdeylins G, Toennies J P and Vollmer R 1989 *12th Symp. Molecular Beams* Abstracts p 98
[21] Jagutzki O, Barnstedt J, Spillmann U, Spielberger L, Mergel V, Ullmann-Pfleger K, Grewing M and Schmidt-Böcking H 1999 *Ultraviolet and X-Ray Detection, Spectroscopy and Polarimetry III (Proc. SPIE vol 3764)* ed S Fineschi, B E Woodgate and R A Kimble pp 61–96
[22] Jardin P, Cassimi A, Grandin J P, Rothard H, Lemoigne J P, Hennecart D, Husson X and Lepoutre A 1995 *Nucl. Instrum. Methods* B **26** 287
[23] Ullrich J, Dörner R, Mergel V, Jagutzki O, Spielberger L and Schmidt-Böcking H 1994 *Comment. At. Mol. Phys.* **30** 285
[24] Mergel V *et al* 1995 *Phys. Rev. Lett.* **74** 2200
[25] Ullrich J, Moshammer R, Dörner R, Jagutzki O, Mergel V, Spielberger L and Schmidt-Böcking H 1997 *J. Phys. B: At. Mol. Opt. Phys.* **30** 2917
[26] Dörner R *et al* 1995 *J. Phys. B: At. Mol. Opt. Phys.* **28** 435
[27] Khayyat Kh *et al* 1999 *J. Phys. B: At. Mol. Opt. Phys.* **32** L73–9
[28] Htwe W T, Vajnai T, Bernhart M, Gaus A D and Schulz M 1995 *Phys. Rev. Lett.* **73** 1348
[29] Shah M D and Gilbody H B 1985 *J. Phys. B: At. Mol. Opt. Phys.* **18** 899
[30] Jardin P, Cassimi A, Grandin J P, Hennecart D and Lemoigne J P 1996 *Nucl. Instrum. Methods* B **107** 41
[31] Unverzagt M, Moshammer R, Schmitt W, Olson R E, Jardin P, Mergel V, Ullrich J and Schmidt-Böcking H 1996 *Phys. Rev. Lett.* **76** 1043
[32] Christenson J H, Cronin J W, Fitch V L and Turlay R 1964 *Phys. Rev. Lett.* **13** 138
[33] Hvelplund P *et al* 1994 *J. Phys. B: At. Mol. Opt. Phys.* **27** 925–34
[34] Moshammer R *et al* 1994 *Phys. Rev. Lett.* **73** 3371
[35] Wood C J and Olson R E 1996 *J. Phys. B: At. Mol. Opt. Phys.* **29** L 257
[36] Crothers D S F and McCann J F 1983 *J. Phys. B: At. Mol. Phys.* **16** 3229
[37] Fainstein P D 1996 *J. Phys. B: At. Mol. Opt. Phys.* **29** L763

[38] O'Rourke S F C and Crothers D S F 1997 *J. Phys. B: At. Mol. Opt. Phys.* **30** 2443

[39] Macek J *et al* 1979 *Phys. Rev.* A **1** 235

[40] Dettmann K, Harrison K G and Lucas M W 1974 *J. Phys. B: At. Mol. Phys.* **7** 269

[41] Meckbach W, Nemirowski I B and Garibotti C R 1981 *Phys. Rev.* A **24** 1793

[42] Garibotti C R and Miraglia J E 1981 *J. Phys. B: At. Mol. Phys.* **14** 863

[43] Macek J, Potter J E, Duncan M M, Menedez M G, Lucas M W and Steckelmacher W 1981 *Phys. Rev. Lett.* **46** 1571

[44] Pregliasco R G, Garibotti C R and Barrachina R O 1994 *J. Phys. B: At. Mol. Opt. Phys.* **27** 1151

[45] Williams E J 1934 *Phys. Rev.* **45** 729
     Jackson J D 1975 *Classical Electrodynamics* (New York: Wiley)

[46] Kristensen F G and Horsdal-Pedersen E 1990 *J. Phys. B: At. Mol. Opt. Phys.* **23** 4129

[47] Kamber E Y, Cocke C L, Cheng S and Varghese S L 1988 *Phys. Rev. Lett.* **60** 2026

[48] Suarez S, Garibotti C, Meckbach W and Bernardi G 1993 *Phys. Rev. Lett.* **70** 418

[49] Dörner R *et al* 1997 *Nucl. Instrum. Methods* B **124** 225

[50] Dörner R, Ullrich J, Olson R E and Schmidt-Böcking H 1989 *Phys. Rev. Lett.* **63** 147

[51] Gensmantel A, Ullrich J, Dörner R, Olson R E, Ullmann K, Forberich E, Lencinas S and Schmidt-Böcking H 1992 *Phys. Rev.* A **45** 4572